The $Fe^{2+}_3(H_2O)_n[PO_4]_2$ Homologous Series.
II. The Crystal Structure of $Fe^{2+}_3(H_2O)[PO_4]_2$

PAUL BRIAN MOORE, AND TAKAHARU ARAKI

Department of the Geophysical Sciences, The University of Chicago,
Chicago, Illinois 60637

Abstract

The synthetic compound $Fe^{2+}_3(H_2O)[PO_4]_2$ has a 9.431(1)Å, b 10.066(1)Å, c 8.040(1)Å, β 117.632(7)°, $P2_1/a$, $Z = 4$. Its structure, refined to $R(hkl) = 0.068$ for 2457 independent reflections, consists of complex open framework formed by edge- and corner-linking of distorted Fe(1) and Fe(3) octahedra, of distorted Fe(2) polyhedra of five-fold oxygen coordination, and of PO_4 tetrahedra. Average bond distances are Fe(1)–O, 2.16 Å; Fe(2)–O, 2.08 Å; Fe(3)–O, 2.15 Å; P(1)–O, 1.55 Å; and P(2)–O, 1.54 Å. Unusual features of the structure include a Fe(2)–P(2) O(6)–O(8) 2.41 Å shared edge; and a Fe(2)–Fe(2)ᶦ O(4)–O(4)ᶦ 2.63 Å shared edge.

It is proposed that a bounded oxidative sequence may exist for the crystal, where $Fe(1)^{2+} \rightarrow Fe(1)^{3+}$ and $H_2O \rightarrow OH-$. The limiting formula for a stable oxidized crystal would be $Fe^{2+}_2 Fe^{3+}(OH)[PO_4]_2$.

Introduction

The homologous series $Fe^{2+}_3(H_2O)_n[PO_4]_2$ includes several compounds where all water molecules and all phosphate oxygens are also bound to the transition metal. Well-characterized natural compounds include vivianite and metavivianite ($n=8$), ludlamite ($n=4$), phosphoferrite ($n=3$), sarcopside and graftonite ($n=0$). In addition, several recently synthesized compounds have been brought to our attention, including the subject of this study, where $n=1$.

Experimental

Single crystals of $Fe^{2+}_3(H_2O)[PO_4]_2$ were synthesized by Dr. E. Mattievich at 230°C and 400 bars pressure, using a hydrothermal technique with synthetic vivianite as starting material. Dr. Mattievich informs us that wet chemical analyses closely conform with the ideal formula and that Mössbauer resonance studies have been performed on the compound.

Preliminary single crystal Weissenberg and precession photographs establish the space group and cell parameters, the latter refined by twelve reflections on the PICKER four-circle automated diffractometer. The results are a 9.431(1) Å, b 10.066(1) Å, c 8.040(1)Å, β 117.632(7)°, space group $P2_1/a$, $Z = 4$. A powder pattern, indexed with the aid of the single crystal data, appears in Table 1.

A superior single crystal measuring 0.09 mm along a, 0.11 mm along b, and 0.04 mm along c was selected for intensity measurements. The compound is pale green in color, with crystals tabular parallel to {001} and striated parallel to [100]. Figure 1 features an idealized sketch of typical development of the crystals.

Successive shells of reflections were gathered to sin $\theta/\lambda = 0.8$ on the PICKER diffractometer with $MoK\alpha_1$ radiation and graphite monochromator. Full scans ranged from 2.4° at the lower levels to 2.8° at high angles with a scan speed of 2°/minute. Twenty-second background measurements were taken on each side of the peak. The data were processed to obtain F(obs) after applying an absorption correction by the Gaussian integral method described by Burnham (1966). All 2457 independent reflections were accepted for the ensuing study.

Structure Determination and Refinements

The Patterson synthesis, $P(uvw)$, revealed that all metals reside in general positions, requiring coordinate determination for Fe(1), Fe(2), Fe(3), P(1), and P(2). Several minimum functions provided unambiguous location of the metals which afforded sufficient scattering matter for a β-general synthesis as described by Ramachandran and Srinivasan (1970). The ensuing map revealed all non-hydrogen atom locations without difficulty.

Full-matrix least-squares refinement, including scale factor, non-hydrogen atomic coordinates and isotropic thermal vibration parameters with 2457 in-

TABLE 1. $Fe_3(H_2O)[PO_4]_2$. Powder Data*

I/I_o	d(obs)	d(calc)	hkl	I/I_o	d(obs)	d(calc)	hkl
70	5.810	5.814	011	20	2.611	2.616	230
20	4.146	4.155	$\bar{1}21$	5	2.571	2.573	$\bar{2}13$
40	4.097	4.100	111	40	2.512	2.517	040
20	3.723	3.730	$\bar{1}12$	5	2.469	2.471	122
10	3.553	3.561	002	20	2.435	2.437	320
100	3.351	3.357	012	5	2.378	2.384	$\bar{3}13$
15	3.030	3.035	031	30	2.324	2.328	$\bar{1}23$
20	2.984	2.992	$\bar{3}11$	10	2.039	2.045	410
15	2.903	2.911	211	20	2.003	2.008	$\bar{2}04$
10	2.722	2.729	112	10	1.894	1.896	123
15	2.680	2.687	131	10	1.833	1.835	$\bar{3}24$
45	2.655	2.659	$\bar{3}21$	10	1.801	1.805	$\bar{1}24$
				15	1.672	1.675	242

*Powder diffractogram, 1°/minute, CuKα radiation, Si ($\underline{a}$ = 5.4301 Å) internal. Indices are based on strong single crystal reflections and cell parameters stated in the text.

dependent reflections converged to $R(hkl) = \Sigma||F(obs)| - |F(calc)||/\Sigma|F(obs)|) = 0.068$. For the 1569 reflections exceeding three times the estimated background error, $R(hkl) = 0.039$. Estimated standard errors in distances are Me–O ± 0.004 Å and O–O′ ± 0.006 Å. Scattering curves for Fe^{1+}, P^0, and O^{1-} derive from the tables of Cromer and Mann (1968).

Final atomic coordinate parameters appear in Table 2, and the structure factor data are presented in Table 3.[1]

Description of the Structure

Topology and Geometry

The crystal structure of $Fe^{2+}_3(H_2O)[PO_4]_2$ is complex, and bears no obvious relationship with any
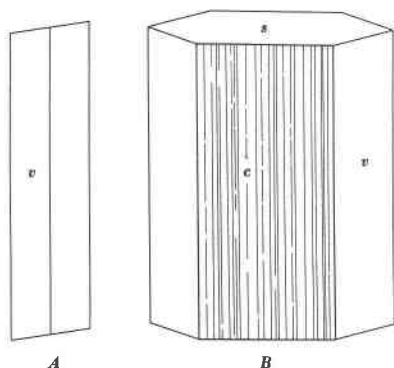
FIG. 1. Typical crystal of $Fe^{2+}_3(H_2O)[PO_4]_2$ showing the forms $c\{001\}$, $v\{011\}$ and $s\{\bar{2}01\}$. A. Plan; B. Clinographic projection.

[1] To receive a copy of Table 3, order document number AM-75-003-A from the Business office, Mineralogical Society of America, 1909 K Street, N.W., Washington, D.C. 20006. Please remit $1.00 for the microfiche.

known structure. There are feeble resemblances to other members of the homologous series, and these relationships shall be emphasized.

To appreciate the problem more fully, we rewrite the formula as a cluster $M^{2+}_2S^{2+}\phi_9$, which consists of three divalent transition metals—two octahedrally coordinated (= M) and one five coordinated (= S)—and nine oxygen-ligand vertices, ϕ, per formula unit. Characteristic of the homologous series $Fe^{2+}_3(H_2O)_n[PO_4]_2$, all n-water molecules are aquated (are found as ligand groups) to the transition metal and all oxygens associated with the $[PO_4]^{3-}$ ligand (= Op) are also bound to transition metals.

In a detailed study on this homologous series certain common characteristics among these structures were emphasized (Moore, 1971). As n decreases, the degree of octahedral condensation or polymerization increases: for n = 8 (vivianite), the octahedral com-

TABLE 2. Atomic Coordinate and Isotropic Thermal Vibration Parameters for $Fe_3(H_2O)[PO_4]_2$*

Atom	x	y	z	B(Å²)
Fe(1)	0.0315(1)	0.1359(1)	0.4130(1)	0.82(1)
Fe(2)	.4386(1)	.8771(1)	.0749(1)	.69(1)
Fe(3)	.2813(1)	.1241(1)	.2628(1)	.61(1)
P(1)	.6740(1)	.0873(1)	.3786(2)	.49(2)
P(2)	.1343(1)	.8320(1)	.0262(2)	.55(2)
O(1)	.8035(4)	.1876(4)	.3950(5)	.72(5)
O(2)	.7485(4)	-.0292(4)	.5172(5)	.67(5)
O(3)	.5430(4)	.1566(4)	.4110(5)	.78(5)
O(4)	.5993(4)	.0308(4)	.1747(5)	.79(5)
O(5)	-.0188(4)	.8713(4)	-.1491(5)	.84(5)
O(6)	.2533(4)	.9497(4)	.1113(5)	.78(5)
O(7)	.0909(4)	.7740(4)	.1723(5)	.91(5)
O(8)	.2342(4)	.7328(4)	-.0255(5)	.81(5)
OW	.0715(4)	.0825(4)	.6840(5)	.98(5)

*Estimated standard errors refer to the last digit.

bination includes the edge-sharing dimer $M_2\phi_{10}$ + the monomer $M\phi_6 = M_3\phi_{16}$, which is equivalent to the expression $\phi_{16} = (H_2O)_8 + (Op)_8$. For $n = 4$ (ludlamite) the cluster formula is $M_3\phi_{12}$ and the structure contains corner-linked chains of $M_3\phi_{14}$ linear edge-sharing trimers bridged by the [PO$_4$] tetrahedra. For $n = 3$ (phosphoferrite), these linear edge-sharing trimers $M_3\phi_{14}$ fuse by further edge- and corner-sharing to form $M_3\phi_{11}$ sheets. For $n = 0$, one of the dimorphs is sarcopside (cf Moore, 1972) which is an ordered derivative of the olivine structure type. With the cluster formula $M_3\phi_8$, we observe the same linear edge-sharing trimers as the structural motif. Since Fe^{2+}_3 $(H_2O)[PO_4]_2$ is compositionally wedged in between, we had anticipated that it, too, would possess these linear edge-sharing trimers.

The $Fe_3(H_2O)[PO_4]_2$ structure not only reveals the absence of such linear trimers, but also provides two kinds of oxygen coordination about the transition metals: two distorted octahedra and one very distorted tetragonal pyramid! In addition, this awkward structure has resisted any obvious vehicle of description, and we despaired of finding a suitable projection until we selected a projection down $\mathbf{a}' = \mathbf{a} - \mathbf{c}$, showing the plane $\mathbf{b} \times \mathbf{c}' \sin \beta'$, where $\mathbf{c}' = \mathbf{a} + \mathbf{c}$. A slab of the structure, where the transition metal coordinates are bounded by $\frac{1}{4} \leq x' \leq \frac{1}{2}$, is provided in Figure 2. This projection, which features the transition metal polyhedra only, has advantages in that all three non-equivalent metals can be referred to a common level in x'. At $x' = \frac{1}{2}$, the polyhedra are stippled, revealing a chain which runs parallel to $\mathbf{c}' \sin \beta'$ with a crankshaft motif. Equivalent chains are further
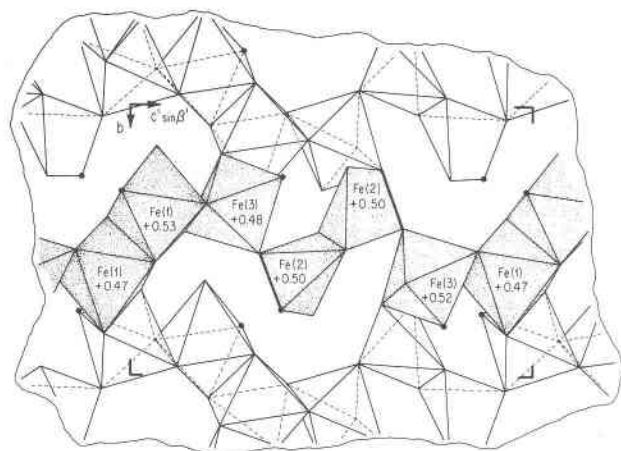
linked above and below to form a highly complex polyhedral framework. The Fe(1)–O octahedron shares three of its edges; one with Fe(1), namely OW^i–OW, and two with Fe(3)'s, namely O(1)–O(3)^{ii} and O(2)^i–O(5)^i. This immediate neighborhood is the $3_6(2)$-cluster of Moore (1974a). The Fe(3)–O octahedron shares two edges with Fe(1) octahedra. Considering only the octahedra, this is the $2_2(2)$ configuration of Moore (1974a). The Fe(2)–O distorted tetragonal pyramids share a mutual edge O(4)–O(4)^i whose center is the center of inversion. In addition, an unanticipated feature, the edge O(6)–O(8) is shared with the P(2)O$_4$ tetrahedron. We feel it necessary and desirable to point out the edge-sharing neighborhoods, for they have considerable implications in homonuclear electron transfer-absorption where the probability of transfer is increased as the distance between metal centers is decreased.

As yet, no theory predicts or explains *a priori* the existence of such an unusual structure. In many respects, the structure is reminiscent of the complex graftonite structure. Although sarcopside is a limiting hexagonal close-packed oxygen structure, the high-temperature dimorph graftonite bears no obvious relationship with it. This unusual structure, as shown by Calvo (1968), possesses three non-equivalent metal positions, two five-coordinated and one seven-coordinated. Despite attempts at several projections, no obvious relationship to $Fe_3(H_2O)[PO_4]_2$ could be found. Unlike $Fe_3(H_2O)[PO_4]_2$, no edges in graftonite are shared between the PO$_4$ tetrahedra and the five-coordinated polyhedra. It is possible that these unusual structures can be rationalized via some sphere-packing theory.

Bond Distances and Angles

Polyhedral interatomic distances are listed in Table 4. The averages for the Fe^{2+}–O octahedral and P–O tetrahedral distances are within the range reported for numerous well-refined structures. The polyhedral interatomic angles in Table 5 reveal rather severe distortions for the octahedra, ranging from O(1)^{ii}–Fe(3)–O(3) 76.9° to O(2)^i–Fe(1)–O(3)^{ii} 116.8°.

The Fe(2)–O polyhedron possesses five vertices, but its angular distortions are so severe that distinction between tetragonal pyramidal and trigonal bipyramidal coordination is not possible. According to the interatomic angle distribution for these two kinds of polyhedra in Stephenson and Moore (1968), the Fe(2)–O polyhedron resembles a trigonal bipyramid with the angle O(4)–Fe(2)–O(8) 170.0° (deviating by 10° from the ideal 180° angle), but most

Fig. 2. Polyhedral diagram of the Fe–O arrangement between $\frac{1}{4} \leq x' \leq \frac{1}{2}$, where $\mathbf{a}' = \mathbf{a} - \mathbf{c}$ and $\mathbf{c}' = \mathbf{a} + \mathbf{c}$. The chain-like character is shown by stippling. Solid disks denote linkages of corners above and below this slab.

TABLE 4. Polyhedral Interatomic Distances for $Fe_3(H_2O)[PO_4]_2$†

Fe(1)		Fe(2)		Fe(3)		P(1)	
Fe(1) $-O(5)^i$	2.070	Fe(2) $-O(7)^{ii}$	1.987	Fe(3) $-O(6)_{ii}$	2.083	P(1)$-O(1)$	1.542
" $-O(3)^{ii}$	2.092	" $-O(6)$	2.036	" $-O(1)_i$	2.135	" $-O(3)$	1.543
" $-OW$	2.101	" $-O(4)_i$	2.052	" $-O(2)_{iii}$	2.140	" $-O(2)$	1.544
" $-O(1)_i$	2.152	" $-O(4)^i$	2.086	" $-O(8)^{iii}$	2.145	" $-O(4)$	1.561
" $-O(2)^i$	2.166	" $-O(8)$	2.243	" $-O(5)^i$	2.206	average	1.548
" $-OW^i$	2.383	average	2.081	" $-O(3)$	2.211		
average	2.161			average	2.153	O(1)$-O(4)$	2.485
						O(2)$-O(4)$	2.517
O(1) $-O(3)^{ii}$	2.703*	Fe(2) $-P(2)$	2.747	O(1)^{ii} $-O(3)_i$	2.703*	O(3)$-O(4)$	2.536
OW $-O(1)_i$	2.731*			O(2)$_i^{ii}$ $-O(5)_{iii}$	2.749*	O(1)$-O(3)$	2.538
O(2)^i $-O(5)_i$	2.749*	O(6) $-O(8)_i$	2.413†	O(1)^{ii} $-O(8)^{iii}$	2.935	O(2)$-O(3)$	2.540
OW^i $-O(5)_i$	2.847	O(4)$_{ii}$ $-O(4)^i$	2.627✓	O(6) $-O(8)^i$	2.947	O(1)$-O(2)$	2.543
OW$_i$ $-O(2)_i$	2.887	O(7) $-O(8)_{ii}$	2.981	O(6)$_{ii}$ $-O(5)^i$	2.975	average	2.526
OW$^i_{ii}$ $-O(2)_i$	2.924	O(4) $-O(7)^{ii}$	3.069	O(1)$^{ii}_{iii}$ $-O(2)^i$	3.031		
O(3)^{ii} $-O(5)^i$	2.951*	O(4)$_i$ $-O(6)$	3.167	O(8)^{iii} $-O(3)_i$	3.084	P(2)	
OW^i $-OW$	3.103	O(4)^i_i $-O(6)$	3.197	O(i)^{ii} $-O(5)^i$	3.100		
OW^i $-O(1)_{ii}$	3.143	O(4)^i $-O(8)_{ii}$	3.364	O(2)^i_i $-O(6)_{iii}$	3.100	P(2)$-O(7)$	1.529
OW $-O(3)_i$	3.353	O(6) $-O(7)^{ii}$	3.514	O(5)^i_i $-O(8)_{iii}$	3.108	" $-O(5)$	1.530
O(1)^i $-O(5)_{ii}$	3.479	average	3.041	O(2)^i $-O(3)$	3.318	" $-O(6)$	1.555
O(2)^i $-O(3)^{ii}$	3.626			O(3) $-O(6)$	3.391	" $-O(8)$	1.556
average	3.041			average	3.037	average	1.542
				Hydrogen Bonds		O(6)$-O(8)$	2.413†
						O(5)$-O(7)$	2.496
				OW $\cdots$ O(7)$_i$	2.72	O(6)$-O(7)$	2.532
				OW $\cdots$ O(7)^i	3.43	O(5)$-O(8)$	2.535
						O(7)$-O(8)$	2.555
						O(5)$-O(6)$	2.571
						average	2.517

† $i = -x, -y, -z$; $ii = 1/2+x, 1/2-y, z$; $iii = 1/2-x, 1/2+y, -z$ applied to coordinate in Table 2.
* Octahedral shared edges.   ‡ Fe(2)-P(2) shared edge.   ✓ Fe(2)-Fe(2)' shared edge.

of the remaining distances more closely resemble the tetragonal pyramid. The Fe(2)–O 2.08 Å average can be compared with the M(2)–O 2.14 and M(3)–O 2.05 Å averages reported by Calvo (1968) for the dis-torted tetragonal pyramid and trigonal bipyramid respectively in graftonite. However, his material contains considerable Mn^{2+} which probably contribute to the longer averages through partial solutions.

TABLE 5. Polyhedral Interatomic Angles for $Fe_3(H_2O)[PO_4]_2$

Fe(1)		Fe(2)		Fe(3)		P(1)	
O(1)$_i$ $-O(3)^{ii}$	79.11°	O(6)$_i$ $-O(8)$	68.47°	O(1)$^{ii}_i$ $-O(3)_i$	76.89°	O(1)$-O(4)$	106.40°
O(5)^i $-OW^i$	79.14	O(4)$^i_{ii}$ $-O(4)$	78.85	O(2)^i_i $-O(5)_i$	78.43	O(2)$-O(4)$	108.29
O(2)^i $-OW^i$	79.84	O(7)$^{ii}_{ii}$ $-O(8)_{ii}$	89.40	O(1)^{ii} $-O(8)^{iii}$	86.60	O(3)$-O(4)$	109.58
O(1)$_i$ $-OW$	79.89	O(4)^i $-O(7)^{ii}$	98.94	O(5)^i $-O(6)_{iii}$	87.82	O(1)$-O(3)$	110.73
O(2)^i_i $-O(5)^i$	80.89	O(4)^i_i $-O(6)$	101.57	O(6) $-O(8)^{iii}$	88.40	O(2)$-O(3)$	110.73
O(2)^i $-OW_i$	85.12	O(4)^i_i $-O(6)$	101.75	O(3)$_{ii}$ $-O(8)^{iii}$	90.15	O(1)$-O(2)$	110.98
OW $-OW^i$	87.32	O(4)^i_i $-O(8)_{ii}$	101.92	O(1)$^{ii}_{ii}$ $-O(2)^i$	90.28		
O(1)$_{ii}$ $-OW^i$	87.62	O(4)^i $-O(7)^{ii}_{ii}$	119.30	O(1)^{ii} $-O(5)_{iii}$	91.11	P(2)	
O(3)^{ii} $-O(5)^i$	90.32	O(6) $-O(7)^{ii}$	136.86	O(5)^i_i $-O(8)$	91.15		
O(3)^{ii} $-OW_i$	106.15	O(4) $-O(8)$	170.00	O(2)^i $-O(6)$	94.43	O(6)$-O(8)$	101.76°
O(1)$_i$ $-O(5)^i_{ii}$	111.02			O(2)^i $-O(3)$	99.35	O(5)$-O(7)$	109.38
O(2)^i $-O(3)^{ii}$	116.77			O(3) $-O(6)$	104.31	O(6)$-O(7)$	110.39
						O(5)$-O(8)$	110.46
						O(7)$-O(8)$	111.83
						O(5)$-O(6)$	112.88

Severe cation-cation repulsion across shared edges results in some very short distances; thus O(6)–O(8), the edge shared by Fe(2) and P(2), equals 2.41 Å, whereas O(4)–O(4)^i, which is shared by two Fe(2), equals 2.63 Å. These distances are the shortest for their polyhedra. Short distances between octahedral shared edges also occur, with the exception of OW–OW^i 3.10 Å. This latter distance reflects the long Fe(1)–OW^i 2.38 Å bond.

Hydrogen Bonds and Electrostatic Valence Balances

The OW molecule can donate two hydrogen bonds with the most likely acceptor being O(7), which coordinates to P(2) and Fe(2) only. Accepting $\xi = +1/6$ for the hydrogen bond strength as suggested by Baur (1970), a model can be found where O(7) accepts one strong and one weak hydrogen bond: OW $\cdots$ O(7) 2.72 Å and OW–O(7)^i 3.43 Å with the angle O(7)–OW–O(7)' 100.1°. Two strong hydrogen bonds would result in a very nearly saturated O(7) anion, since $\Sigma = 5/4+2/5+1/6+1/6 = 1.98$. Since Fe(2)–O(7) and P(2)–O(7) are the shortest distances for their polyhedra, the presence of one feeble bond is more likely.

The remaining anions deviate only slightly from saturation by cations and accordingly show no systematic deviations in their Me–O bond distances. All oxide anions associated with Fe(1) are slightly un-

FIG. 3. The links between the Fe atoms where edges are shared. This diagram follows from Figure 2. Arrows, pointing in the plane and above or below, denote edge-links.

dersaturated with $\Delta\Sigma = -0.08$, adding further support to the likely preferential oxidation at the Fe(1) site discussed below.

A Proposed Oxidation Sequence for Fe$^{2+}_3$(H$_2$O)[PO$_4$]$_2$

Moore (1971) has pointed out that only certain compositions in the homologous series Fe$^{2+}_3$(H$_2$O)$_n$[PO$_4$]$_2$ are capable of continuous oxidation of the metals without destruction of the structure. The compositions are limited by the condition of maintenance of local electrostatic neutrality of cations about anions during oxidation. Permissible bonded units include H$_2$O-bridged ferrous ions (as in edge-sharing Fe^{2+} octahedra) where Fe^{2+} (OH$_2$)$_2$Fe^{2+} can be continuously oxidized to hydroxide-bridged ferric ions—Fe^{3+}(OH)$_2$Fe^{3+}. On the other hand, hydroxide-bridged ferrous ions, Fe^{2+}(OH)$_2$Fe^{2+}, lead to extreme oxygen undersaturation. Analogously, such species as Fe^{3+}(OH) or Fe^{3+}(OH$_2$)Fe^{3+} also lead to local charge balance difficulties and are, accordingly, not observed. Of the homologous series, only $n = 3$ is capable of continuous oxidation to a stable ferric end-member since permissible end-member combinations are preserved. Thus, the series Fe$^{2+}_3$(H$_2$O)$_3$[PO$_4$]$_2$ (phosphoferrite) — Fe$^{3+}_3$(OH)$_3$[PO$_4$]$_2$ (kryzhanovskite) is observed in Nature; the others decompose to yield essentially amorphous ferric equivalents after progressive and complete oxidation (Moore, 1971). A more recent study on pure synthetic phosphoferrite and its ferric equivalent has established beyond doubt the existence of both ferrous and ferric end-member compositions belonging to the same structure type when the hydrogen atom positions are excluded (Moore, 1974b).

Since Fe^{2+}(OH$_2$)$_2$Fe^{2+} ions occur in Fe$^{2+}_3$(H$_2$O)[PO$_4$]$_2$, we propose that a bounded mixed valence composition can occur as a stable crystal. The mid-point of the OW–OW' edge shared between two Fe(1) atoms is an inversion center. This suggests that an upper bound for a stable oxidized equivalent would be Fe$^{2+}_2$Fe^{3+}(OH)[PO$_4$]$_2$, where Fe(1) is completely oxidized.

If such an oxidative sequence does indeed exist, then mixed-valence transfer and intense pleochroism should occur with maximum absorption along the Fe(1)$^{3+}$—Fe(3)$^{2+}$ direction. Unique Fe–Fe separations across the shared edges are Fe(1)–Fe(1) 3.25 Å, Fe(1)–Fe(3) 3.11 and 3.20 Å, and Fe(2)–Fe(2) 3.20 Å. We provide a skeleton of Fe–Fe' connections and distances across shared edges in Figure 3. These distances are similar to those found between the

shared edge in vivianite, suggesting that mild oxidation of $Fe^{2+}_3(H_2O)[PO_4]_2$ would result in intense pleochroism, similar to that observed for vivianite.

References

BAUR, W. H. (1970) Bond length variation and distorted coordination polyhedra in inorganic crystals. *Trans. Am. Crystallogr. Assoc.* **6,** 129–155.

BURNHAM, C. W. (1966) Computation of absorption corrections, and the significance of the end effect. *Am. Mineral.* **51,** 159–167.

CALVO, C. (1968) The crystal structure of graftonite. *Am. Mineral.* **53,** 742–750.

CROMER, D. T., AND J. B. MANN (1968) X-ray scattering factors computed from numerical Hartree-Fock wave functions. *Acta Crystallogr.* **A24,** 321–324.

MOORE, P. B. (1971) The $Fe^{2+}_3(H_2O)_n(PO_4)_2$ homologous series: crystal-chemical relationships and oxidized equivalents. *Am. Mineral.* **56,** 1–7.

—— (1972) Sarcopside: its atomic arrangement. *Am. Mineral.* **57,** 24–35.

—— (1974a) Structural hierarchies among minerals containing octahedrally coordinating oxygen II. Systematic retrieval and classification of octahedral edge-sharing clusters: an epistemological approach. *Neues Jahrb. Mineral. Abh.* **120,** 205–227.

—— (1974b) Evidence for a complete mixed valence solid solution series in $Fe^{2+}_3(H_2O)$ $[PO_4]_2$ (phosphoferrite)—$Fe^{3+}_3(OH)_3[PO_4]_2$ (kryzhanovskite). *Nature, Phys. Sci.* **251,** 305.

RAMACHANDRAN, G. N., AND R. SRINIVASAN (1970) *Fourier Methods in Crystallography.* Wiley-Interscience, New York, p. 96–119.

STEPHENSON, D. A., AND P. B. MOORE (1968) The crystal structure of grandidierite, $(Mg,Fe)Al_3SiBO_9$. *Acta Crystallogr.* **B24,** 1518–1522.